Journal of Materials Chemistry B

RSC Publishing

PAPER

View Article Online
View Journal | View Issue

Cite this: *J. Mater. Chem. B*, 2013, **1**, 1133

Photothermally enhanced photodynamic therapy based on mesoporous Pd@Ag@*m*SiO_2 nanocarriers†

Saige Shi, Xianglong Zhu, Zengxia Zhao, Weijun Fang, Mei Chen, Yizhuan Huang and Xiaolan Chen*

Received 7th November 2012
Accepted 17th December 2012

DOI: 10.1039/c2tb00376g

www.rsc.org/MaterialsB

In this work, we have demonstrated that mesoporous silica-coated Pd@Ag nanoparticles (Pd@Ag@*m*SiO_2) can be used as an excellent nanoplatform for photodynamic therapy (PDT) drug delivery. Photosensitizer molecules, Chlorin e6 (Ce6), are covalently linked to the mesoporous shell and the prepared Pd@Ag@*m*SiO_2–Ce6 nanoparticles exhibit excellent water solubility, good stability against leaching and high efficiency in photo-generating cytotoxic singlet oxygen. More importantly, the photothermal effect of Pd@Ag nanoplates under the irradiation of a NIR laser can enhance the uptake of Pd@Ag@*m*SiO_2–Ce6 nanoparticles by cells, further increasing the PDT efficiency toward cancer cells. The photothermally enhanced PDT effects were demonstrated both *in vitro* and *in vivo*. When the Pd@Ag@*m*SiO_2–Ce6 nanoparticles were injected intratumorally into the S180 tumor-bearing mice, the tumors were completely destroyed without recurrence of tumors upon irradiation with both 808 nm and 660 nm lasers, while the irradiation with 808 nm or 660 nm alone did not. These results indicate that the Pd@Ag@*m*SiO_2 nanoparticles may be a valuable new tool for application in cancer phototherapy.

1 Introduction

Photodynamic therapy (PDT) has emerged as an important therapeutic modality for various diseases, including cancer.[1] PDT is based on the concept that photosensitizers (PSs) interact with molecular oxygen to generate reactive oxygen species, such as singlet oxygen ($^1O_2$), upon proper light irradiation for the killing of cancer cells.[1–4] However, the application of many PSs in the clinic has been limited by their nonspecific damage to normal tissues, environmental degradation, and poor water solubility, which highly reduce PDT efficacy.[5] To overcome these problems, various delivery systems have been developed for effective delivery of PSs.[5–22] Among them, mesoporous silica nanoparticles (MSNs) are promising candidates as platforms for PDT applications due to their outstanding properties of high surface area, tunable pore size, excellent biocompatibility, versatile surface modification and avid cell uptake.[15–22] The large surface areas and porous matrix structures of MSNs not only allow significant numbers of PSs to be conveyed, but also help to improve the diffusivity of ground state O_2 that interacts with the PSs for effective singlet oxygen generation.

In addition to develop various carrier vehicles, another means of enhancing the PDT therapeutic efficacy is by combining PDT with other treatment modalities,[13,14,22–25] *e.g.* hyperthermia.[23–25] Hyperthermia, a procedure of raising the temperature of tumour-loaded tissue to 40–43 °C, has been used as an adjunctive therapy with other established cancer treatments such as chemotherapy.[26–33] Although the clinical hyperthermia methods in which the heat is usually provided by incubation chambers, radiowave irradiation or limb perfusion, can improve the therapeutic effect of chemotherapy drugs, however, undesirable side effects to normal organs are also induced due to the nonspecific site heating.[28–30] Recently hyperthermia produced by near-infrared (NIR) absorbing photothermal nanomaterials such as gold nanoparticles,[31,32,34,35] carbon nanotubes,[36,37] graphene,[38] CuS/Cu_{2-x}Se nanocrystals[39] and Pd nanoplates[40–42] have been extensively investigated in cancer photothermal therapy (PTT). These nanomaterials can strongly absorb NIR light and convert it into heat for site-specific killing of cancer cells. A gold nanorod–photosensitizer complex has been developed for noninvasive near-infrared fluorescence imaging and PTT/PDT dual therapy *in vivo*.[24] It has also been demonstrated that the photothermal effect of graphene can be utilized to promote the delivery of photosensitizer molecule, Chlorin e6 (Ce6), by mild local heating under the

Department of Chemistry, College of Chemistry and Chemical Engineering, Xiamen University, Xiamen 361005, China. E-mail: chenxl@xmu.edu.cn; Tel: +86-592-2186437

† Electronic supplementary information (ESI) available: N_2 adsorption/desorption isotherm and the pore size distribution of nanoparticles, FTIR spectra, absorption spectra, Zeta potentials, visible/NIR spectra, temperature *versus* time plots of solutions containing Pd@Ag@*m*SiO_2–Ce6 nanoparticles, trypan blue stained images of HeLa cells incubated with Pd@Ag@*m*SiO_2–Ce6 nanoparticles, flow cytometry measurements, temperature change of the tumor site, IR images of the tumor sites, summary of the treatments applied to mice for comparative therapeutic efficacy study. See DOI: 10.1039/c2tb00376g

irradiation of lower power NIR laser upon graphene oxide (GO)–PEG–Ce6 nanoparticles, further enhancing the cancer cell killing during PDT treatment against cancer cells.[25] These results motivated us to further explore other NIR absorbing nanomaterials for photothermally enhanced PDT efficacy.

Owing to their high optical absorption in the near infrared region and excellent photothermal stability, Pd@Ag nanoplates can effectively absorb and convert NIR light into heat.[41,42] Recently we have reported the synthesis of mesoporous silica-coated Pd@Ag nanoparticles (denoted as Pd@Ag@sSiO$_2$@m-SiO$_2$ or Pd@Ag@mSiO$_2$) loaded with anti-cancer drug, doxorubicin (DOX). These nanoparticles showed a synergistic effect of combining chemotherapy and photothermal therapy *in vitro* under NIR irradiation.[42]

Here we demonstrate that the Pd@Ag@mSiO$_2$ nanoparticles can be used as an excellent nanocarrier for the photosensitizer, Ce6, through covalent bonding (Scheme 1). The large pores and high surface area in the mesoporous shell facilitate covalent grafting of the PSs onto the rigid porous structure, which in turn not only increases their water solubility and stability, avoids degradation and premature release into the systemic circulation in harsh biological environment, but also helps to improve the accumulation of the PS drugs in the tumor site, thereby enhancing the PDT efficacy.[19,21,22] The obtained Pd@Ag@m-SiO$_2$–Ce6 nanoparticles exhibit high efficiency in photogenerating cytotoxic singlet oxygen under the irradiation with a 660 nm laser at 0.1 W cm^{-2} power density. At the meantime, the mild heating effect produced from the Pd@Ag nanoplates can increase cellular membrane permeability for enhanced drug uptake by cells.[43] We observed the Pd@Ag@mSiO$_2$–Ce6 nanoparticles-treated cells displaying stronger intracellular fluorescence from Ce6 under the irradiation of 808 nm NIR laser than without irradiation by both confocal microscope and flow cytometer. These Pd@Ag@mSiO$_2$–Ce6 nanoparticles were injected intratumorally into the S180 tumor-bearing mice, the tumors were completely destructed without recurrence upon irradiation at 808 nm and 660 nm simultaneously. Our data clearly showed that a synergism of photo and thermal effect of Pd@Ag@mSiO$_2$–Ce6 nanoparticles was able to enhance the delivery of PDT agents and improve the efficiency of photodynamic cancer cell killing.

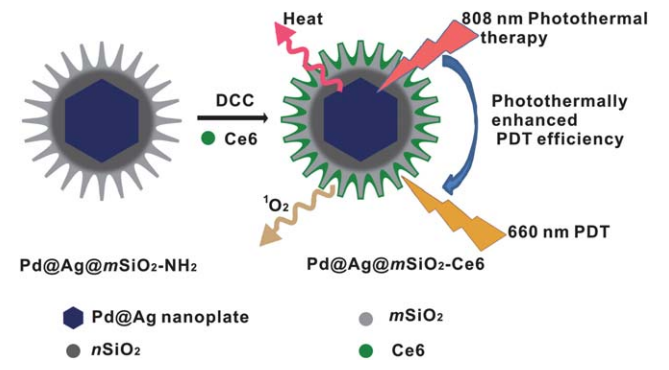

Scheme 1 Schematic image showing how to load Ce6 into Pd@Ag@mSiO$_2$ nanoparticles and use them for PDT.

2 Experimental section

2.1 Materials

All chemicals were obtained from commercial suppliers and used without further purification. Pd(acac)$_2$, tetraethoxysilane (TEOS), 3-aminopropyltriethoxysilane (APTES) and trimethylbenzene were purchased from Alfa Aesar. L-Arginine (Arg) and dodecyltrimethylammonium chloride (CTAC) were obtained from Sinopharm Chemical Reagent Co., Ltd. (Shanghai). *N*,*N*-Dicyclohexylcarbodiimide (DCC) and 1,3-diphenylisobenzofuran (DPBF) were purchased from Sigma-Aldrich. Chlorin e6 (Ce6) was received from J&K Scientific Ltd. (Beijing).

2.2 Characterization

The scanning electron microscopy (SEM) images were taken by using a Hitachi S4800 scanning electron microscope with a field emission electron gun. Transmission electron microscopy (TEM) images were obtained using a TECNAI F-30 high resolution transmission electron microscope operating at 300 kV. UV/Vis absorption spectra were measured with a Cary 5000 UV/Vis/NIR spectrophotometer (Varian). Dynamic light scattering (DLS) and zeta-potential experiments were carried out on a Nano-ZS (Malvern Instruments).

2.3 Preparation of Pd@Ag@mSiO$_2$ nanoparticles

The Pd@Ag@mSiO$_2$ nanoparticles were synthesized by a multi-step method according to our recently reported protocol with slight modifications.[42] First, Pd@Ag nanoplates (~41 nm in diameter) were prepared according to the procedure reported previously.[41] And then a layer of dense silica were coated onto Pd@Ag nanoplates using a modified Stöber method. Typically, 6.17 mg of Pd@Ag nanosheets were dispersed in 128 ml of ethanol, and 320 μl of TEOS and 2.0 ml of methylamine aqueous solution (40%) were added in sequence. The mixture were stirred at room temperature for 10 h, and then nanoparticles was recovered *via* centrifugation at 14 500 rpm for 12 minutes, washed three times and re-dispersed in ethanol.

The final step is to coat a layer of mesoporous silica on the above prepared nanoparticles.[44] Typically, the above prepared nanoparticles were re-dispersed in 120 ml of ultrapure water in the presence of CTAC (480 mg) and trimethylbenzene (1.2 ml) and ultrasonicated for 30 min. 160 μl of TEOS and 24.0 mg of Arg (L-arginine) were added into the solution. After stirring at 45 °C for 24 h, the as-prepared nanoparticles were collected by centrifugation and washed several times with ethanol–water mixed solution. The collected Pd@Ag@mSiO$_2$ nanoparticles were finally re-dispersed in ammonium nitrate ethanol solution (1.2 g of NH_4NO_3 in 60 ml ethanol) at 45 °C for 18 h to thoroughly remove the surfactant template.

2.4 Preparation of Pd@Ag@mSiO$_2$–NH$_2$

Porous silica coating was modified with amine groups in order to covalently link PSs. In a typical procedure, 30.0 mg of Pd@Ag@mSiO$_2$ nanoparticles were dispersed in 60.0 ml ethanol, and 60.0 μl water and 30.0 μl 3-aminopropyltriethoxysilane

(APTES) were added. The mixture was then aged at 45 °C for overnight under magnetic stirring. The resulting Pd@Ag@*m*-SiO_2–NH_2 nanoparticles were collected by centrifugation and washed three times with ethanol for further use.

2.5 Preparation of Pd@Ag@*m*SiO_2–Ce6

N,*N*-Dicyclohexylcarbodiimide (DCC) was used as the condensing agent to ensure that the carboxylic groups of Chlorin e6 (Ce6) selectively reacted with the amino groups of Pd@Ag@*m*SiO_2–NH_2 in *N*,*N*-dimethylformamide (DMF). 10 mg of Ce6, 15 mg of DCC and 10 mg of Pd@Ag@*m*SiO_2–NH_2 nanoparticles were added to a 3.0 ml DMF solution. The mixture was stirred at room temperature for 24 h. The obtained Pd@Ag@*m*SiO_2–Ce6 nanoparticles were purified through centrifugation and washed with DMF for three times. The supernatant which contained unreacted Ce6 molecules was collected and used to determine the amount of Ce6 loaded onto the Pd@Ag@*m*SiO_2–NH_2 nanoparticles by measuring the intensity of UV/Vis spectra at 404 nm.

2.6 Detection of singlet oxygen ($^1O_2$)

We used a chemical probe 1,3-diphenylisobenzofuran (DPBF) to assess the capability of Pd@Ag@*m*SiO_2–Ce6 nanoparticles for singlet oxygen ($^1O_2$) generation.[45] DPBF can react irreversibly with $^1O_2$ that causes a decrease in the DPBF absorption at around 400 nm. In a typical experiment, 20 μl of DPBF (1.5 mg ml^{-1} in acetonitrile) was added into 800 μl ethanol which contains a proper amount of Pd@Ag@*m*SiO_2–Ce6 nanoparticles. The solutions were then irradiated with a 660 nm laser at the light power density of 0.1 W cm^{-2}, and the absorbance at 413 nm was recorded at different periods of time. The corresponding absorption of Pd@Ag@*m*SiO_2–Ce6 nanoparticles at 413 nm was deducted.

2.7 Cell culture and cellular uptake

HeLa cell line was obtained from the cell storeroom of Chinese Academy of Science and grown in RPMI-1640 culture medium containing 10% calf serum and 1% penicillin/streptomycin at 37 °C under 5% CO_2. To test the uptake of Pd@Ag@*m*SiO_2–Ce6 nanoparticles, HeLa cells were plated in 35 mm culture dishes at a density of about 1×10^5 cells per dish in RPMI-1640. After culturing for 24 h, the cell medium was replaced by fresh medium containing 40 μg ml^{-1} of Pd@Ag@*m*SiO_2–Ce6 nanoparticles or the same amount of free Ce6, and incubated for different periods of time (4 and 8 h). After washing the cells with PBS, fluorescence imaging was performed on an Olympus Fluoview 1000 laser-scanning microscope.

For the NIR light-promoted the uptake of HeLa cell on Pd@Ag@*m*SiO_2–Ce6 nanoparticles, HeLa cells were first incubated with 40 μg ml^{-1} of nanoparticles for 2 h. After washing off the unbound nanoparticles, the cells at 37 °C were irradiated by 808 nm laser (0.4 W cm^{-2}) for 15 min or incubated at 42 °C in the dark for 15 min. After another 2 h incubation, confocal images of cells were taken.

2.8 Cytotoxicity of the Pd@Ag@*m*SiO_2–Ce6 nanoparticles

For the cell toxicity assay, HeLa cells were pre-cultured in a 96-well plate at 1×10^4 per well for 24 h and then added with Pd@Ag@*m*SiO_2–Ce6 nanoparticles at a series of concentrations. After incubation for 12 h, cell viabilities were measured by using the standard MTT (3-(4,5)-dimethylthiahiazo-2-yl)-2,5-diphenyltetrazolium bromide) assay.

2.9 Photodynamic effect of the Pd@Ag@*m*SiO_2–Ce6 nanoparticles on HeLa cells

For MTT assay, HeLa cells were seeded in 96-well cell culture plates at a density of 1×10^4 per well for 24 h. Then the medium was replaced by 200 μl cell medium containing Pd@Ag@*m*SiO_2–Ce6 nanoparticles at 90 or 120 μg ml^{-1}. After incubation for 12 h, the cells were washed three times with PBS and subjected to different lasers irradiation for 5 min. After another 4 h incubation, the standard MTT assay was carried out to determine the cell viabilities.

For optical imaging, HeLa cells were grown in a 24-well cell culture plate at a density of $\sim 0.5 \times 10^5$ cells per well for 24 h. Then 90 or 120 μg ml^{-1} of Pd@Ag@*m*SiO_2–Ce6 nanoparticles were added and incubated for 12 h. After irradiation by different lasers for 5 min, the cells were stained with 0.04% trypan blue solution for 3 min. Microscopic images of cells were then recorded using a fluorescence microscope.

2.10 Therapeutic efficacy of Pd@Ag@*m*SiO_2–Ce6 nanoparticles in S180 tumor-bearing mice

Female Kunming mice (~20 g) used in this study were provided from Laboratory Animal Center of Xiamen University. All experiments were operated according to the Animal Management Rules of the Ministry of Health of the People's Republic of China and the guidelines for the Care and Use of Laboratory Animals of China. The S180 tumor model was established by subcutaneously injecting S180 cells ($\sim 2 \times 10^6$) into the right rear legs in the mice. When the tumor grew to a diameter of ~7 mm, the mice were separated into five groups (five mice per group) and intratumorally injected with ~125 μl of PBS or 125 μl of Pd@Ag@*m*SiO_2–Ce6 nanoparticles (150 μg ml^{-1}). The tumors were irradiated with the 660 nm laser (0.1 W cm^{-2}), 808 nm laser (1 W cm^{-2}), or both of them for 5 min. After treatment, the tumor volume was calculated as length × $(width)^2 \times 1/2$ with a caliper every two days. The relative tumor volume was calculated as V/V_0, V_0 and V stand for the tumor volume on the initial day and on the day of measurement, respectively.

2.11 *In vivo* NIR imaging

The S180 tumor-bearing mice were intratumorally injected with 125 μl of PBS or 125 μl of Pd@Ag@*m*SiO_2–Ce6 nanoparticles at 150 μg ml^{-1}. The tumor on each mouse was exposed to the 808 nm laser with a power density of 1 W cm^{-2} for 5 min, an infrared thermography (HM-300, Guangzhou SAT Infrared Technology Co., Ltd.) was used to capture the temperature change on the site of the tumor.

3 Results and discussion

3.1 Synthesis and characterization of Pd@Ag@mSiO$_2$–Ce6 nanoparticles

The mesoporous silica-coated Pd@Ag nanoparticles (Pd@Ag@mSiO$_2$) were fabricated following our recently reported procedures,[42] and loaded with photosensitizer Ce6, through covalent bonds (Scheme 1).

As shown in Fig. 1a and c, the as-prepared Pd@Ag@mSiO$_2$ nanoparticles had an average diameter of ~141 nm with Pd@Ag nanoplates (~41 nm) encapsulated in a one-in-one fashion. Obvious large pores were observed in the mesoporous shells due to the use of trimethylbenzene (TMB) as a swelling agent for the CTAC micelles to enlarge the pores. The large pore feature was also confirmed by the N_2 adsorption/desorption measurements (Fig. S1†).

After reacting with 3-aminopropyltriethoxysilane (APTES), the Pd@Ag@mSiO$_2$ nanoparticles were modified with amino groups. These amine-bearing particles were then crosslinked with photosensitizer Ce6, through a covalent conjugation strategy in which *N*,*N*-dicyclohexylcarbodiimide (DCC) was used as the condensing agent to ensure that the carboxylic groups of Ce6 selectively reacted with the amino groups of Pd@Ag@mSiO$_2$–NH$_2$ nanoparticles in DMF. The successful grafting of Ce6 onto the nanoparticles was confirmed by the UV/Vis absorption spectra in Fig. 2. From the UV/Vis spectra of the Pd@Ag@mSiO$_2$–Ce6 nanoparticles, the characteristic Ce6 absorption peaks were clearly identified (Fig. 2a). Based on the difference of absorption intensity at 404 nm between the feeding Ce6 concentration and the supernatant solution which was obtained by centrifuging the reaction solution of Pd@Ag@mSiO$_2$–NH$_2$ and Ce6 (Fig. S3†), the loading of Ce6 was calculated to be about 25 wt% with respect to the Pd@Ag@mSiO$_2$–NH$_2$ nanoparticles.

After loading Ce6 onto the Pd@Ag@mSiO$_2$, the morphologies and sizes of Pd@Ag@mSiO$_2$–Ce6 nanoparticles were similar to those of Pd@Ag@mSiO$_2$ (Fig. 1b and d). The size distribution of Pd@Ag@mSiO$_2$–Ce6 nanoparticles measured by dynamic light scattering (DLS) is approximately 164 nm (Fig. 2b), which is a little larger than that measured from TEM (Fig. 1d). The as-prepared Pd@Ag@mSiO$_2$–Ce6 nanoparticles were well dispersed in aqueous solution and remained stable (Fig. 2c). Owing to the robust covalent bond between Ce6 and Pd@Ag@mSiO$_2$–NH$_2$, it is expected that Ce6 has a low chance of leaking from the Pd@Ag@mSiO$_2$–Ce6 nanoparticles when incubated in biological environments for a long time. As expected, after storing for two months in phosphate-buffered saline (PBS, pH 7.4), the nanoparticles were centrifuged and the absorption of the supernatant was measured. As shown in Fig. 2d, only ~3.3% dye leakage from the nanoparticles was observed, suggesting that Pd@Ag@mSiO$_2$–Ce6 nanoparticles are very stable against dye leaching. The good stability gives these nanoparticles the potential for various biological applications. In addition, the zeta-potentials of Pd@Ag@mSiO$_2$, Pd@Ag@mSiO$_2$–NH$_2$ and Pd@Ag@mSiO$_2$–Ce6 nanoparticles in aqueous solutions at pH 7.4 were measured to be −31.3 mV, 8.24 mV and −4.86 mV (Fig. S4†), respectively.

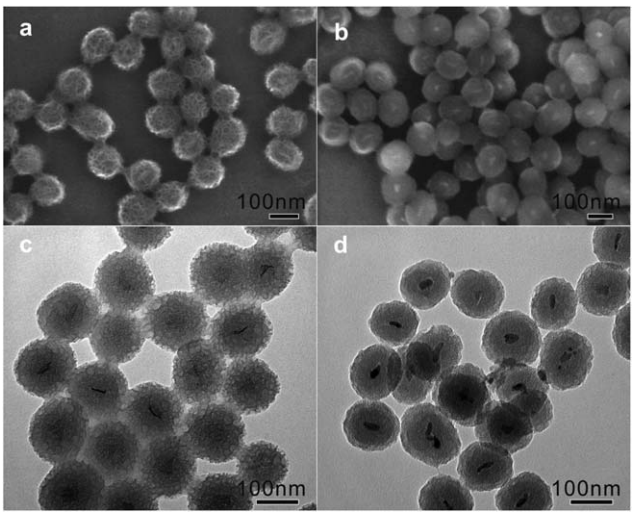

Fig. 1 SEM and TEM images of Pd@Ag@mSiO$_2$ (a and c) and Pd@Ag@mSiO$_2$–Ce6 (b and d) nanoparticles.

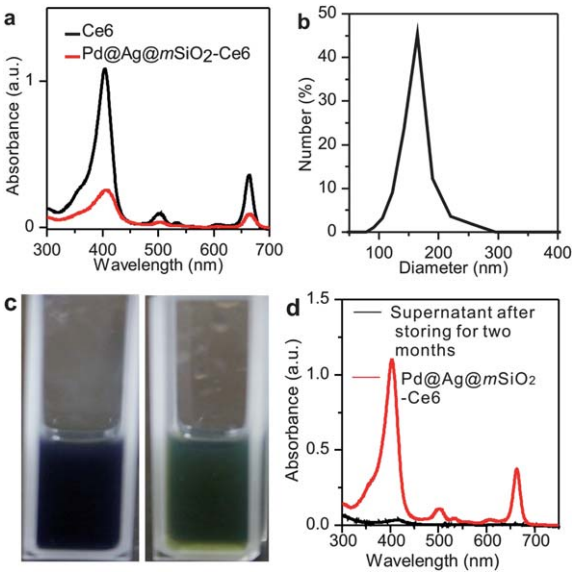

Fig. 2 (a) Absorption spectra of free Ce6 and Pd@Ag@mSiO$_2$–Ce6 nanoparticles. (b) Size distribution of Pd@Ag@mSiO$_2$–Ce6 nanoparticles in water. (c) Photographs of Pd@Ag@mSiO$_2$–NH$_2$ and Pd@Ag@mSiO$_2$–Ce6 nanoparticles in PBS. (d) Absorption spectra of Pd@Ag@mSiO$_2$–Ce6 nanoparticles after storing for two months and the supernatant by centrifugation.

3.2 Singlet oxygen production from the Pd@Ag@mSiO$_2$–Ce6 nanoparticles

Singlet oxygen generation is the key step in photodynamic killing of cancer cells. To verify the production of singlet oxygen ($^1O_2$) by the Pd@Ag@mSiO$_2$–Ce6 nanoparticles, 1,3-diphenylisobenzofuran (DPBF) was employed as a probe molecule. DPBF reacts irreversibly with $^1O_2$ and the reaction can be monitored by measuring the decrease in DPBF absorption intensity at ~400 nm.[45] As shown in Fig. 3a, the absorption spectra of DPBF

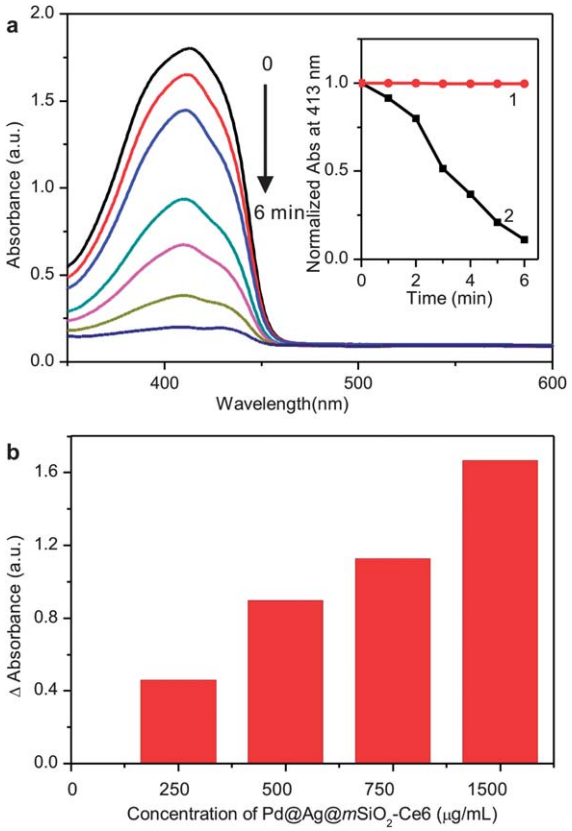

Fig. 3 (a) Absorption spectra of DPBF in the presence of Pd@Ag@mSiO$_2$–Ce6 nanoparticles after irradiation for different times with a 660 nm laser source at 0.1 W cm^{-2}. Inset: decay curves of DPBF absorption at 413 nm as a function of irradiation time. (1) DPBF and (2) DPBF with Pd@Ag@mSiO$_2$–Ce6 nanoparticles solution. (b) Concentration dependence decrease in DPBF absorption (ΔA) by Pd@Ag@mSiO$_2$–Ce6 nanoparticles under the 660 nm laser irradiation, measurement time for 2 min.

gradually decreased with 660 nm (0.1 W cm^{-2}) irradiation in the presence of Pd@Ag@mSiO$_2$–Ce6 nanoparticles, suggesting an increased amount of $^1O_2$ produced by the Ce6-conjugated nanoparticles. In contrast, the absorption of DPBF almost remained unchanged in the absence of Pd@Ag@mSiO$_2$–Ce6 nanoparticles under the same experimental conditions (see Fig. 3a inset), confirming that the decrease in absorption of DPBF was a result of the combined effect of Pd@Ag@mSiO$_2$–Ce6 and the light irradiation. It is also interesting to find that the generation of $^1O_2$ from the Pd@Ag@mSiO$_2$–Ce6 nanoparticles is concentration-dependent, more $^1O_2$ will be produced as the nanoparticle concentrations increase (Fig. 3b). The excellent $^1O_2$ generation capacity by the Pd@Ag@mSiO$_2$–Ce6 nanoparticles inspires us to apply them in PDT treatment of cancer cells.

3.3 Cytotoxicity, cell uptake and *in vitro* PDT studies on HeLa cells under irradiation from a 660 nm laser

Before applying these nanoparticles for the photodynamic killing of cancer cells, the biocompatibility and cell uptake capacity of the Pd@Ag@mSiO$_2$–Ce6 nanoparticles were first examined by the 3-(4,5-dimethylthiazol-2-yl)-2,5-diphenyltetrazolium bromide (MTT) assay and fluorescence microscope image, respectively. As shown in Fig. 4a, upon incubation with Pd@Ag@mSiO$_2$–Ce6 nanoparticles in the range of 0–500 μg ml^{-1} for 12 h, the cellular viability of HeLa cells still remained above 75%. The MTT results indicated that the Pd@Ag@mSiO$_2$–Ce6 nanoparticles had low cell-cytotoxicity and good biocompatibility.

To monitor the intracellular uptake of the Pd@Ag@mSiO$_2$–Ce6 nanoparticles, HeLa cells were incubated with the Pd@Ag@mSiO$_2$–Ce6 nanoparticles (40 μg ml^{-1}) for 4 and 8 h at 37 °C. After washing the unbound nanoparticles, images of the cells were taken with a confocal fluorescence microscope (Fig. 4d and e). As shown in Fig. 4d and e, the intense red fluorescence of Ce6 was observed inside the cells and the fluorescence increased over incubation time. In comparison, the intracellular fluorescence signals were much weaker when HeLa cells were incubated with the same concentrations of free Ce6 for 4 or 8 h (Fig. 4b and c). The improved Ce6 delivery efficacy by

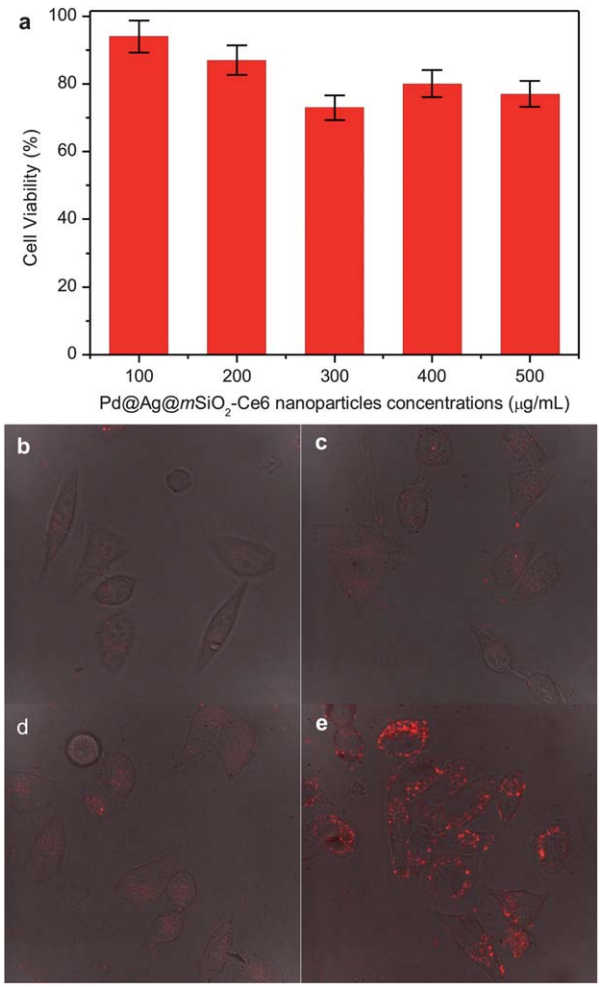

Fig. 4 (a) Viability of HeLa cells incubated for 12 h with different concentrations of Pd@Ag@mSiO$_2$–Ce6 nanoparticles. Confocal fluorescence images of HeLa cells incubated with free Ce6 (b and c) and Pd@Ag@mSiO$_2$–Ce6 (d and e) for 4 h (b and d) and 8 h (c and e), respectively. The concentration of nanoparticles was 40 μg ml^{-1} (~16.7 μM Ce6).

the Pd@Ag@mSiO$_2$–Ce6 nanoparticles was probably due to the ease of endocytosis of the nanoparticles by cancer cells.[42] The increased uptake of Ce6-loaded Pd@Ag@mSiO$_2$ nanoparticles by the cancer cells is a prerequisite for PDT treatment.

The *in vitro* PDT effects of the Pd@Ag@mSiO$_2$–Ce6 nanoparticles upon HeLa cells were assessed by both MTT assay and trypan blue staining experiments. After incubation with Pd@Ag@mSiO$_2$–Ce6 nanoparticles at two different concentrations of 90 and 120 μg ml^{-1} for 12 h, the nanoparticles treated cells were irradiated with a 660 nm laser at a power density of 0.1 W cm^{-2} for 5 min and incubated for an additional 4 h. Compared to the control groups without light irradiation, the cell viabilities in the 660 nm light irradiated groups decreased ~13% (Fig. 5a) for 90 μg ml^{-1} and ~22% (Fig. 5b) for 120 μg ml^{-1} of Pd@Ag@mSiO$_2$–Ce6 nanoparticles, respectively.

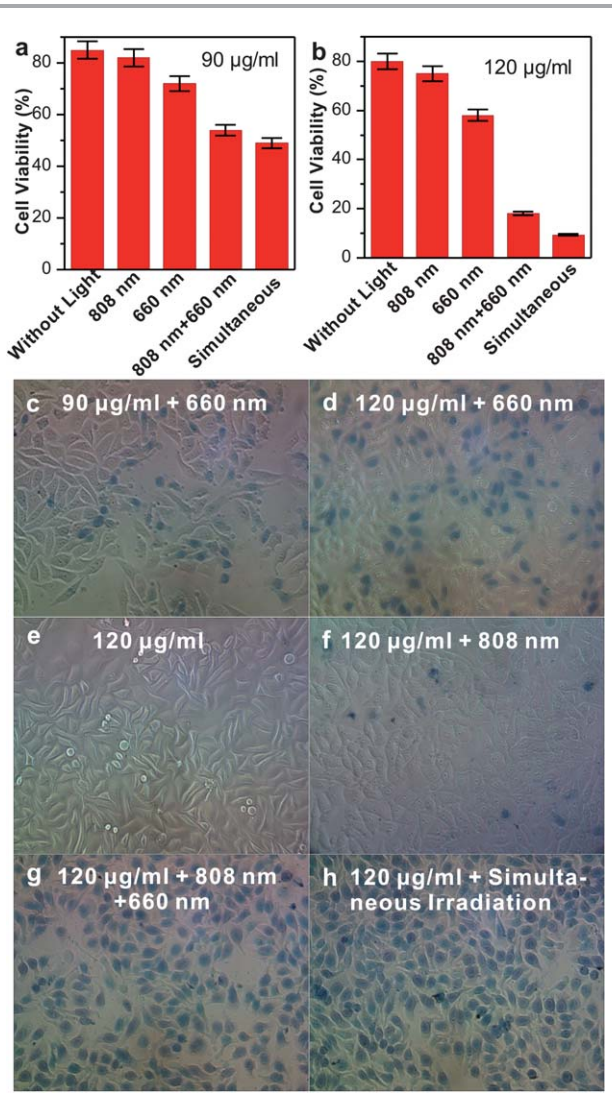

Fig. 5 *In vitro* photodynamic and photothermally enhanced cancer cell killing. (a and b) cell viability data of HeLa cells incubated with Pd@Ag@mSiO$_2$–Ce6 at 90 μg ml^{-1} (a) and 120 μg ml^{-1} (b) after various laser treatments. Trypan blue stained images of HeLa cells incubated with Pd@Ag@mSiO$_2$–Ce6 nanoparticles at 90 μg ml^{-1} with 660 nm laser irradiation (c) and 120 μg ml^{-1} (d–h) with various laser treatments. The power densities for 660 nm and 808 nm lasers are 0.1 W cm^{-2} and 1 W cm^{-2}, respectively.

Microscopic images of trypan blue stained cells further confirmed that the Pd@Ag@mSiO$_2$–Ce6 nanoparticles had good photodynamic cancer cells killing capacity (Fig. 5c and d).

3.4 Photothermally enhanced PDT effects

Pd@Ag nanoplates can strongly absorb NIR light and convert it into heat. As shown in Fig. S5,† after silica coating, the strong NIR absorption feature of Pd@Ag nanoplates was maintained well. The Ce6-loaded Pd@Ag@mSiO$_2$ nanoparticles displayed obvious photothermal conversion effects in aqueous solution upon irradiation with a 1 W laser at 808 nm (Fig. S6†). The temperature of the solution containing 200 μg ml^{-1} Pd@Ag@mSiO$_2$–Ce6 nanoparticles was raised from 27 to 38.8 °C after irradiation for 10 min, while the temperature almost remained unchanged for the deionized water or free Ce6 solution. Therefore, it is expected that the good NIR light absorption capacity of the Pd@Ag@mSiO$_2$–Ce6 nanoparticles can be utilized to enhance the photodynamic killing efficacy of cancer cells. To test this, HeLa cells were first incubated with Pd@Ag@mSiO$_2$–Ce6 nanoparticles at two concentrations of 90 and 120 μg ml^{-1} for 12 h. After washing with PBS to remove the unbound nanoparticles, the cells were subjected to the following handling: (1) irradiated with an 808 nm NIR laser (1 W cm^{-2}) for 5 min; (2) first irradiated with an 808 nm NIR laser (1 W cm^{-2}) for 5 min which was able to induce a temperature increase of ~6 °C, then the 660 nm laser (0.1 W cm^{-2}) for 5 min (denoted as 808 nm + 660 nm); (3) simultaneously irradiated with the 808 nm laser (1 W cm^{-2}) and 660 nm laser (0.1 W cm^{-2}) for 5 min (denoted as simultaneous irradiation or simultaneous). Microscopy images of HeLa cells after different treatments are shown in Fig. 5 and S7.† Compared to cells irradiated with the 660 nm laser (0.1 W cm^{-2}) alone (Fig. 5c and d), irradiation with 808 nm and 660 nm laser in turn (Fig. 5g and S7d†) or simultaneous irradiation (Fig. 5h and S7e†) demonstrated an increased cell death at all test concentrations. It was worth noting that 808 nm laser irradiation (1 W cm^{-2}, 5 min) by itself induced no obvious cell death in the Pd@Ag@mSiO$_2$–Ce6 nanoparticle treated cells (Fig. 5f and S7c†). The relative cell viabilities for the above investigations were also measured after PDT treatments. The results agreed with those from the fluorescence microscopy experiments. With the 808 nm NIR light prior or simultaneous irradiation with the 660 nm laser, the cell viabilities further reduced (Fig. 5a and b). For example, with the NIR light prior to irradiation, ~31% and 62% of cell growth inhibitions were achieved for the 90 and 120 μg ml^{-1} of Pd@Ag@mSiO$_2$–Ce6 nanoparticles, respectively, while with the simultaneous irradiation, even higher cell growth inhibitions of 36% and 71% were observed at concentrations of 90 and 120 μg ml^{-1} Pd@Ag@mSiO$_2$–Ce6 nanoparticles cases respectively (Fig. 5a and b). These results indicated that adding NIR light irradiation can greatly enhance the toxicity of Pd@Ag@mSiO$_2$–Ce6 nanoparticles, causing more cell death than nanoparticles with only 660 nm laser irradiation.

There are two possible reasons for the increased cell death. One is the synergistic effects of photothermal and photodynamic therapy, the other is the photothermally enhanced the

PDT efficiency. As mentioned above, the 808 nm laser irradiation (1 W cm^{-2}, 5 min) alone caused no obvious cell death to Pd@Ag@*m*SiO_2–Ce6 nanoparticles treated cells, whether the residual heat generated by 808 nm laser irradiation causing cells death or not, two other control experiments were conducted to elucidate this. First, the Pd@Ag@*m*SiO_2–Ce6 nanoparticle treated HeLa cells were left at room temperature for 30 min to cool down after the 808 nm laser irradiation, and then the 660 nm laser irradiation was applied. It was found that the cell death rate was similar with that of without staying at room temperature for 30 min (Fig. S8a and b†). In the second control experiment, the Pd@Ag@*m*SiO_2–Ce6 nanoparticle treated HeLa cells were firstly irradiated by 660 nm laser for 5 min, then 880 nm laser for 5 min (results are shown in the ESI, Fig. S8d†), no obvious increased cell death rate was observed in comparison with cells treated by 660 nm laser alone (Fig. S8c†). Therefore, we concluded that 808 nm laser irradiation can greatly improve photodynamic killing cancer cells.

To find out why the 808 nm laser irradiation can enhance the PDT efficacy, we first investigated the cell uptake of the Pd@Ag@*m*SiO_2–Ce6 nanoparticles with the 808 nm laser irradiation, which increased the temperature to about 42 °C, and without by confocal fluorescence imaging. As shown in Fig. 6, brighter red fluorescence was observed inside the cells after the 808 nm laser irradiation (Fig. 6b) compared to cell samples without irradiation (Fig. 6a), indicating more Pd@Ag@*m*SiO_2–Ce6 nanoparticles were taken up by the cells. In addition, it was found that increasing the incubation temperature to 42 °C using a water bath also led to the enhanced uptake of Pd@Ag@*m*SiO_2–Ce6 by cells (Fig. 6c). Ce6 fluorescence from cells measured by flow cytometry further confirmed that the increased cellular uptake of Pd@Ag@*m*SiO_2–Ce6 by 808 nm laser irradiation (Fig. 6d and S9†). With 808 nm laser irradiation, the fluorescence of Ce6 is 1.3 times greater than that cells incubated with Pd@Ag@*m*SiO_2–Ce6 without laser irradiation. These results might be explained that the NIR light irradiation induced local heating of Pd@Ag@*m*SiO_2–Ce6 nanoparticles that are close to the cell membrane can increase the temperature of nanoparticles-treated cells, further increased cell membrane permeability and led to the improved cellular uptake of Pd@Ag@*m*SiO_2–Ce6 nanoparticles which generated more $^1O_2$ for killing cancer cells. Our data clearly evidenced that the photothermal effect of Pd@Ag@*m*SiO_2–Ce6 nanoparticles was able to enhance the delivery of PDT agents for improved photodynamic cancer cell killing.

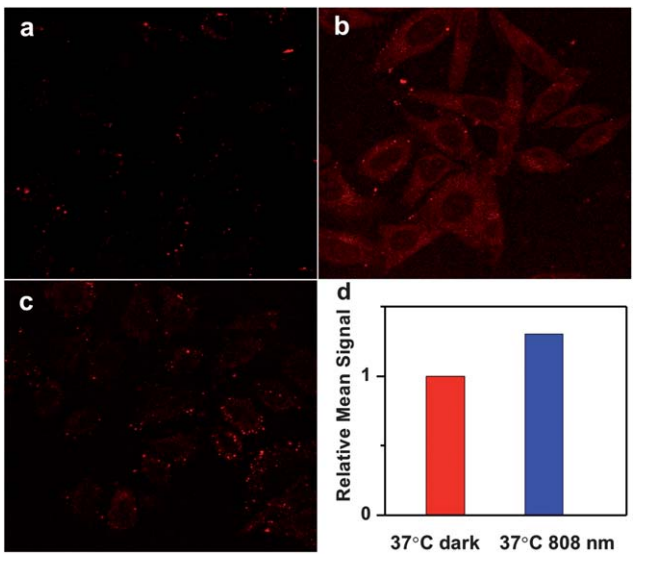

Fig. 6 Photothermally enhanced delivery of Ce6 by Pd@Ag@*m*SiO_2 nanoparticles. (a–c) Confocal images of HeLa cells incubated with Pd@Ag@*m*SiO_2–Ce6 at 37 °C with (b) or without (a) 808 nm laser irradiation (0.4 W cm^{-2}, 15 min) and cells incubated at 42 °C in the dark (c) for 15 min. (d) The mean fluorescent signal of cells treated with Pd@Ag@*m*SiO_2–Ce6 with 808 nm laser irradiation for 15 min or not obtained from flow cytometry measurements.

3.5 *In vivo* therapeutic efficacy of Pd@Ag@*m*SiO_2–Ce6 in tumor-bearing mice

To investigate the therapeutic efficacy of Pd@Ag@*m*SiO_2–Ce6 nanoparticles upon S180 tumor-bearing mice under different laser irradiation, comparative efficacy studies were carried out. We divided the S180 tumor-bearing mice into five groups ($n = 5$, where n is the number of mice in each group) and treated them with the protocols that were listed in Table S1.† Photographs of the mice taken before, 3 days and 7 days after different light irradiation and the relative tumor volume change *versus* time for each group are presented in Fig. 7. As shown in Fig. 7a, the mice treated with PBS under the simultaneous irradiation of 808 nm and 660 nm lasers (group 1) displayed tumor volume increasing with time (black line in Fig. 7a). However, irradiation of the tumor region by both 808 nm and 660 nm lasers after injection of Pd@Ag@*m*SiO_2–Ce6 remarkably suppressed tumor growth (pink line in Fig. 7a and b). The tumor volume was rapidly reduced and completely disappeared after 7 days. Though irradiation by 660 nm laser or 808 nm laser alone after injection the Pd@Ag@*m*SiO_2–Ce6 nanoparticles also suppressed tumor growth to a certain degree at the initial period, the tumor began to grow again at the later stage (blue and green lines in Fig. 7a and b), implying that the incomplete destruction of tumors cells by the photodynamic or photothermal treatment can induce a recurrence of the tumor. Furthermore, the Pd@Ag@*m*SiO_2–Ce6 nanoparticles had no inhibitory effect on tumor growth without light irradiation (red line in Fig. 7a), suggesting that the nanoparticles could not produce cytotoxic ROS or heat to inhibit tumor growth without light irradiation. These results further revealed that the photodynamic treatment effect of Pd@Ag@*m*SiO_2–Ce6 nanoparticles can be improved by the 808 nm NIR light irradiation.

It should be pointed out that compared to *in vitro* cell experiment, better photothermal therapeutic effect of Pd@Ag@*m*-SiO_2–Ce6 nanoparticles was obtained in the *in vivo* study when the tumor was illuminated with 808 nm laser. First, the different amounts of accumulated Pd@Ag@*m*SiO_2–Ce6 nanoparticles between *in vitro* cells and *in vivo* tumor tissues may affect the therapy outcome, since the photothermal conversion efficiency is correlated with the concentration of nanoparticles. In our experiment, the *in vitro* photothermal cell study was performed after washing the nanoparticles, the net temperature increase

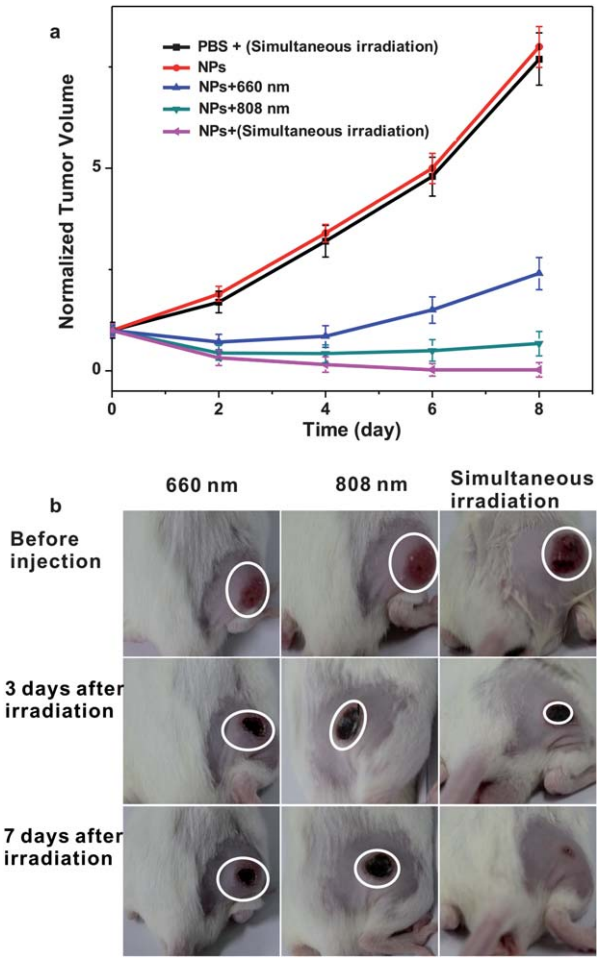

Fig. 7 (a) Relative tumor volume change *versus* time for the mice treated with PBS and Pd@Ag@mSiO$_2$–Ce6 nanoparticles with different light irradiation, respectively (n = 5). (b) Photographs of the Pd@Ag@mSiO$_2$–Ce6 nanoparticles treated mice taken before, 3 days and 7 days after different laser irradiation.

was about 6 °C (the room temperature was about 33 °C), which resulted in minimal therapeutic effects. While at the tumor tissue, after intratumoral injecting the Pd@Ag@mSiO$_2$–Ce6 nanoparticles, almost all the plasmonic nanomaterials accumulated in the tumor sites, as a result, the temperature increased about 16 °C (from 27 to 43 °C) of the tumor tissues (Fig. S10 and S11†). Temperature rise of ~16 °C would partly inhibit the growth of tumor tissue (Fig. 7a). In addition, photothermal therapy causing tumor vascular endothelial cell injury, vascular repair ability decline and comparatively lower oxygen level and pH in cancer cells also might contribute to the better therapy effects *in vivo*.[46,47] Therefore, better *in vivo* therapy effect was achieved than that of *in vitro* therapy.

4 Conclusions

In summary, Pd@Ag@mSiO$_2$ nanoparticles were applied as nanocarriers for the photosensitizer Ce6 for photothermally enhanced photodynamic therapy studies. The Ce6 covalently conjugated to the mesoporous silica shell exhibit excellent stability against leaching and good efficiency in photogenerating of reactive oxygen species. Due to the increased cellular uptake of Ce6 delivered by the Pd@Ag@mSiO$_2$ nanoparticles, in which the Pd@Ag nanoplates can convert the NIR light to heat under NIR laser irradiation, the PDT efficacy of Pd@Ag@mSiO$_2$–Ce6 nanoparticles was greatly enhanced by irradiation with both 808 nm and 660 nm lasers together. The prominent antitumor effects of the Pd@Ag@mSiO$_2$–Ce6 nanoparticles on the S180 tumor-bearing mouse model demonstrated the promising prospect of Pd@Ag@mSiO$_2$ as a potential drug delivery system for *in vivo* PDT-mediated cancer therapy.

Acknowledgements

We thank professor Nanfeng Zheng for helpful discussions and comments on the manuscript. We also thank Dr Jianli Zou at Kyoto University for help with proofreading, Dr Binghui Wu for help with the images, Dr Shaoheng Tang for help with the IR images and Dr Guoliang Ke for help with the flow cytometry experiments. The work was supported by the National Natural Science Foundation of China (no. 21101131), Natural Science Foundation of Fujian Province (no. 2012J01056), Fundamental Research Funds for the Central Universities (2010121015), Scientific Research Foundation for the Returned Overseas Chinese Scholars of State Education Ministry.

Notes and references

1 M. Triesscheijn, P. Baas, J. H. M. Schellens and F. A. Stewart, *Oncologist*, 2006, **11**, 1034.
2 D. E. J. G. J. Dolmans, D. Fukumura and R. K. Jain, *Nat. Rev. Cancer*, 2003, **3**, 380.
3 L. R. Braathen, R. M. Szeimies, N. Basset-Seguin, R. Bissonnette, P. Foley, D. Pariser, R. Roelandts, A. M. Wennberg and C. A. Morton, *J. Am. Acad. Dermatol.*, 2007, **56**, 125.
4 J. P. Celli, B. Q. Spring, I. Rizvi, C. L. Evans, K. S. Samkoe, S. Verma, B. W. Pogue and T. Hasan, *Chem. Rev.*, 2010, **12**, 2795.
5 Y. N. Konan, R. Gruny and E. Allémann, *J. Photochem. Photobiol., B*, 2002, **66**, 89.
6 B. Chen, B. W. Pogue and T. Hasan, *Expert Opin. Drug Delivery*, 2005, **2**, 477.
7 T. Y. Ohulchanskyy, I. Roy, L. N. Goswami, Y. H. Chen, E. J. Bergey, R. K. Pandey, A. R. Oseroff and P. N. Prasad, *Nano Lett.*, 2007, **7**, 2835.
8 D. K. Chatterjee, L. S. Fong and Y. Zhang, *Adv. Drug Delivery Rev.*, 2008, **60**, 1627.
9 X. X. He, X. Wu, K. M. Wang, B. H. Shi and H. Luo, *Biomaterials*, 2009, **30**, 5601.
10 P. Zhang, W. Steelant, M. Kumar and M. Scholfield, *J. Am. Chem. Soc.*, 2007, **129**, 4526.
11 J. Schwiertz, A. Wiehe, S. Gräfe, B. Gitter and M. Epple, *Biomaterials*, 2009, **30**, 3324.
12 Y. Cheng, A. C. Samia, J. D. Meyers, I. Panagopoulos, B. Fei and C. Burda, *J. Am. Chem. Soc.*, 2008, **130**, 10643.
13 H. W. Gu, K. M. Xu, Z. M. Yang, C. K. Chang and B. Xu, *Chem. Commun.*, 2005, 4270.

14 C. L. Peng, M. J. Shieh, M. H. Tsai, C. C. Chang and P. S. Lai, *Biomaterials*, 2008, **29**, 3599.
15 S. H. Cheng, C. H. Lee, C. S. Yang, F. G. Tseng, C. Y. Mou and L. W. Lo, *J. Mater. Chem.*, 2009, **19**, 1252.
16 R. R. Zhang, C. L. Wu, L. L. Tong, B. Tang and Q. H. Xu, *Langmuir*, 2009, **25**, 10153.
17 S. H. Cheng, C. H. Lee, M. C. Chen, J. S. Souris, F. G. Tseng, C. S. Yang, C. Y. Mou, C. T. Chen and L. W. Lo, *J. Mater. Chem.*, 2010, **20**, 6149.
18 H. S. Qian, H. C. Guo, P. C. L. Ho, R. Mahendran and Y. Zhang, *Small*, 2009, **5**, 2285.
19 T. T. Zhao, H. Wu, S. Q. Yao, Q. H. Xu and G. Q. Xu, *Langmuir*, 2010, **26**, 14937.
20 J. Zhu, H. X. Wang, L. Liao, L. Z. Zhao, L. Zhou, M. H. Yu, Y. H. Wang, B. H. Liu and C. Z. Yu, *Chem.–Asian J.*, 2011, **6**, 2332.
21 F. Wang, X. L. Chen, Z. X. Zhao, S. H. Tang, X. Q. Huang, C. H. Lin, C. B. Cai and N. F. Zheng, *J. Mater. Chem.*, 2011, **21**, 11244.
22 T. T. Wang, L. Y. Zhang, Z. M. Su, C. G. Wang, Y. Liao and Q. Fu, *ACS Appl. Mater. Interfaces*, 2011, **3**, 2479.
23 M. F. Zhang, T. Murakami, K. Ajima, K. Tsuchida, A. S. D. Sandanayaka, O. Ito, S. Lijima and M. Yudasaka, *Proc. Natl. Acad. Sci. U. S. A.*, 2008, **105**, 14773.
24 B. Jang, J. Y. Park, C. H. Tung, I. H. Kim and Y. Choi, *ACS Nano*, 2011, **5**, 1086.
25 B. Tian, C. Wang, S. Zhang, L. Z. Fang and Z. Liu, *ACS Nano*, 2011, **5**, 7000.
26 G. M. Hahn, J. Braun and I. Har-kedar, *Proc. Natl. Acad. Sci. U. S. A.*, 1975, **72**, 937.
27 J. Overgaard, *Cancer Res.*, 1976, **36**, 3077.
28 D. L. Fraker, H. R. Alexander, M. Andrich and S. A. Rosenberg, *J. Clin. Oncol.*, 1996, **14**, 479.
29 P. Wust, B. Hildebrand, G. Screenivasa, B. Rau, J. Gellermann, H. Riess, R. Felix and P. M. Schlag, *Lancet Oncol.*, 2002, **3**, 487.
30 F. K. Storm, W. H. Harrison, R. S. Elliott and D. L. Morton, *Cancer Res.*, 1979, **39**, 2245.
31 S. M. Lee, H. Park and K. H. Yoo, *Adv. Mater.*, 2010, **22**, 4049.
32 J. H. Park, G. von Maltzahn, L. L. Ong, A. Centrone, T. A. Hatton, E. Ruoslahti, S. N. Bhatia and M. J. Sailor, *Adv. Mater.*, 2010, **22**, 880.
33 S. P. Sherlock, S. M. Tabakman, L. M. Xie and H. J. Dai, *ACS Nano*, 2011, **5**, 1505.
34 J. Y. Chen, D. L. Wang, J. F. Xi, L. Au, A. Siekkinen, A. Warsen, Z. Y. Li, H. Zhang, Y. N. Xia and X. D. Li, *Nano Lett.*, 2007, **7**, 1318.
35 X. H. Huang, I. H. El-Sayed, W. Qian and M. A. El-Sayed, *J. Am. Chem. Soc.*, 2006, **128**, 2115.
36 H. K. Moon, S. H. Lee and H. C. Choi, *ACS Nano*, 2009, **3**, 3707.
37 X. Liu, H. Tao, K. Yang, S. Zhang, S. T. Lee and Z. Liu, *Biomaterials*, 2011, **32**, 144.
38 K. Yang, S. Zhang, G. Zhang, X. Sun, S. T. Lee and Z. Liu, *Nano Lett.*, 2010, **10**, 3318.
39 D. Dorfs, T. Härtling, K. Miszta, N. C. Bigall, M. R. Kim, A. Genovese, A. Falqui, M. Povia and L. Manna, *J. Am. Chem. Soc.*, 2011, **133**, 11175.
40 X. Q. Huang, S. H. Tang, X. L. Mu, Y. Dai, G. X. Chen, Z. Y. Zhou, F. X. Ruan, Z. L. Yang and N. F. Zheng, *Nat. Nanotechnol.*, 2011, **6**, 28.
41 X. Q. Huang, S. H. Tang, B. J. Liu, B. Ren and N. F. Zheng, *Adv. Mater.*, 2011, **23**, 3420.
42 W. J. Fang, J. Yang, J. W. Gong and N. F. Zheng, *Adv. Funct. Mater.*, 2012, **22**, 842.
43 P. Shen, J. Hawksworth, J. Lovato, B. W. Loggie, K. R. Geisinger, R. A. Fleming and E. A. Levine, *Ann. Surg. Oncol.*, 2004, **11**, 178.
44 T. Yokoi, T. Karouji, S. Ohta, J. N. Kondo and T. Tatsumi, *Chem. Mater.*, 2010, **22**, 3900.
45 W. Spiller, H. Kliesch, D. Wohrele, S. Hackbarth, B. Roder and G. J. Schnurpfeil, *J. Porphyrins Phthalocyanines*, 1998, **2**, 145.
46 Y. Tang and A. J. McGoron, *J. Photochem. Photobiol., B*, 2009, **97**, 138.
47 Y. Sawaji, T. Sato, A. Takeuchi, M. Hirata and A. Ito, *Br. J. Cancer*, 2002, **86**, 1597.